

The impact of insolation, greenhouse gas forcing and ocean circulation changes on glacial inception

The Holocene
21(5) 803–817
© The Author(s) 2011
Reprints and permission:
sagepub.co.uk/journalsPermissions.nav
DOI: 10.1177/0959683610394885
hol.sagepub.com


G. Vettoretti and W.R. Peltier

University of Toronto, Canada

Abstract

In this study we employ the NCAR CCSM3 coupled model to investigate the onset of high northern latitude perennial snow cover. Two periods of Earth's insolation history, that of the pre-industrial period and that of 116 ka before present (BP), are used as benchmarks in an investigation of the influences of interglacial greenhouse gas (GHG) concentration and insolation upon the occurrence of permanent summer snow cover. An additional two experiments at 10 ka and 51 ka into the future (AP) using a typical interglacial GHG level are used to investigate the length of the current interglacial. Results from this set of multicentury sensitivity experiments demonstrate the relative importance of forcings due to insolation and atmospheric greenhouse gases at the millennial scale, and of Atlantic ocean overturning strength (AMOC) at the century scale. We find that while areas of perennial snow cover are sensitive to GHG concentrations, they are much more sensitive to the contemporaneous insolation regime. The goodness of fit of the climatology of the control model to the modern observed climatology is found to influence the modeling results. While there is a strong correlation between AMOC decadal variability and high latitude surface temperature in our control climates, we find little change in AMOC strength during our simulations of 116 ka BP climate nor do we find significant correlation between high latitude snow accumulation and the AMOC. Both the 10 ka AP and 51 ka AP future simulations produce inception events which are much stronger than that of the equivalent pre-industrial simulation. The simulation of inception at 10 ka into the future suggests a maximum duration of the current interglacial of approximately 20 ka in the absence of modern anthropogenic forcing.

Keywords

early anthropogenic hypothesis, glacial inception, greenhouse gas concentrations, Holocene, ocean circulation

Introduction

Late Quaternary climate variability is directly linked to the changes in the geometry of the Earth's orbit around the Sun. Slow variations of the eccentricity of the orbit itself, of the obliquity of the spin-axis with respect to the normal to the plane of the ecliptic, and of the interaction of these elements with the precession of the equinoxes influenced the seasonal distribution of received insolation and thereby exerted a strong influence upon climate evolution. These changes in the seasonal distribution of insolation are well established as primary components involved in the onset and termination of Northern Hemisphere ice-sheet evolution during the second half of the Quaternary (Deblonde and Peltier, 1991a, b; Hays et al., 1976; Milankovitch, 1941; Shackleton et al., 1990; Tarasov and Peltier, 1999).

The transition between interglacial and glacial conditions is characterized by the rapid increase of continental land ice volume at high latitudes, as indicated by the rapid fall in sea level inferred from the geological record during such transitions (Andrews and Mahaffy, 1976). For example, the eustatic sea-level fall at the end of the last interglacial during Marine Isotope Stage (MIS) 5d is thought to have exceeded 20 m in 5000 yr (e.g. Waelbroeck et al., 2002), with the majority of this water being invested in the formation of the Laurentide Ice Sheet. The rapid accumulation of high northern latitude perennial snow cover occurs as a result of ice-albedo feedback during periods of extremely low Northern Hemisphere summer seasonal insolation

(Milankovitch, 1941; see Claussen et al., 2007 for a summary review). After several centuries of perennial snow cover, when conditions result in accumulation exceeding ablation throughout the year, vast expanses of these northern regions will become ice-covered as the snow is compacted under its own weight. Additional feedback processes, such as that involving a southward shift of the tundra–taiga biome boundary, ocean circulation changes, and atmospheric circulation changes have all been proposed as possible mechanisms involved in the acceleration of the glacial inception process (Calov et al., 2005, 2009; Crucifix and Loutre, 2002; De Noblet et al., 1996; Desprat et al., 2005; Gallimore and Kutzbach, 1996; Kageyama et al., 2004; Khodri et al., 2001; Meissner et al., 2004; Vettoretti and Peltier, 2003b). The influence of the concentrations of well-mixed greenhouse gases (GHG) present in the atmosphere during periods of glacial inception has also been proposed as a forcing mechanism that may play a role in snow accumulation. Previous studies have found that GHG forcing plays a secondary role to insolation forcing in

Received 16 June 2010; revised manuscript accepted 26 November 2010

Corresponding author:

G. Vettoretti, Department of Physics, University of Toronto, 60 St George Street, Toronto ON, M5S 1A7, Canada
Email: g.vettoretti@utoronto.ca

the accumulation of high latitude perennial snow cover (e.g. Calov et al., 2009; Vettoretti and Peltier, 2004). In this issue, Vavrus et al. (2011) investigate the role of topography in the same model used in this study but with the T42 and T85 atmosphere coupled to a slab ocean model. Their results, which are similar to those obtained in this study (at T42) indicate that the higher resolution almost doubles the amount of perennial snow cover at high latitudes.

The early anthropogenic hypothesis

The hypothesis that increased human agricultural production altered the natural interglacial trends in CO₂ and CH₄ during the latter part of the Holocene is an intriguing notion (Ruddiman, 2003). If humans did in fact begin to significantly alter the climate as much as 8000 years ago, this may have had significant implications for both the onset of a next glacial cycle and for the future impact that humans will have on the climate system under increasing GHG concentrations (Claussen et al., 2005). Ruddiman (2003, 2006, 2007) suggested that various forms of early human activity, including rice cultivation, animal herding and land-use change significantly increased the GHG concentrations of the atmosphere. Ruddiman (2007) suggests that the CO₂ and CH₄ concentrations in the atmosphere just prior to this 'pre-industrial' revolution would have achieved a level of approximately 240 ppmv and 450 ppbv, respectively. These values are estimated based on the conjecture that through human activity over the past 8000 years, the CO₂ and CH₄ concentrations were actually increased by approximately 40 ppmv and 250 ppbv, respectively. The additional radiative forcing associated with these increases is hypothesized to have prevented the onset of a next glacial cycle. Ruddiman (2008) furthermore argues that the four natural factors proposed for GHG concentration increases during the last 8000 years (net carbon storage on land, ocean carbonate compensation, ocean temperature and coral reef construction) cannot account for the observed Holocene CO₂ changes.

At no time in the past half million years have interglacial CO₂ levels reached as low a level as 240 ppmv except for a brief period during MIS 7 at 238 ka BP (Figure 1; Lüthi et al., 2008). The same holds true for CH₄ concentrations of 450 ppbv (Figure 1; Loulergue et al., 2008). These recorded CO₂ levels appear to be discordant with the claim proposed by the early anthropogenic hypothesis that CO₂ levels should have reached 240 ppmv during the Holocene. During MIS 7, eccentricity is at 4% and the precessional and obliquity forcing are in phase and so promote strong Northern Hemisphere summer seasonal cooling within 15 000 years of the preceding deglaciation event (see discussion below). MIS 11, a much closer analogue for the present rather than is the MIS 7 interglacial, was characterized by atmospheric CO₂ concentration between 270 and 290 ppmv for no less than 20 000 years. Likewise, atmospheric CH₄ concentrations are between 500 and 700 ppbv for the first half of MIS 11. It is highly probable on the basis of these comparisons that CO₂ and CH₄ concentrations would have remained in excess of 260 ppmv and 550 ppbv, respectively, during the entire Holocene period and likely for another 10 000 years in the absence of modern anthropogenic forcing.

Broecker et al. (1999, 2001) have suggested that the ocean carbonate compensation mechanism was responsible for increases in GHG concentrations from the start of the Holocene until the

pre-industrial period. Broecker and Stocker (2006) furthermore argue that because of the multimillennial timescale involved, the oceans would have had time to equilibrate with the increases in early anthropogenic GHG concentrations, thus requiring five times the amount of CO₂ release proposed by Ruddiman (2003) to raise the levels of GHG observed to have occurred during the latter part of the Holocene. Instead they argue that the increase in GHG concentrations during the latter part of the Holocene is a result of a readjustment in oceanic carbonate chemistry. They associate the initial decreases of GHGs in the beginning of the Holocene with uptake of GHGs due to the expansion of high latitude peat bogs and forests as the Northern Hemisphere ice sheets receded following deglaciation. This drawdown in GHG concentrations during the early Holocene would have increased the carbonate ion concentration in the ocean and thereby caused the lysocline to deepen. During the ensuing 8000 years, the CaCO₃ accumulation on the sea floor would exceed the rate of supply and reduce the carbonate ion concentration of the ocean resulting in a readjustment of the lysocline with a time constant of approximately 5000 years. The inverse relationship between pCO₂ and carbonate ion concentration requires that the atmospheric CO₂ concentration rise in response to the readjustment process. According to Broecker et al. (1999), if the carbonate compensation mechanism was in fact operational, the δ¹³C isotopic concentration of the atmosphere recorded in ice core records would remain constant.

Elsig et al. (2009) present a highly resolved atmospheric δ¹³C isotope record of the past 11 000 years from measurements of atmospheric CO₂ trapped in the EPICA Dome C (EPICA Community Members, 2004) ice core. Through detailed inverse mass-balance modelling that permits an analysis of the atmosphere–ocean and atmosphere–land carbon fluxes, their study indicates that the initial changes in δ¹³C from 11 ka BP to 8 ka BP are the result of land-biosphere uptake as suggested by Broecker et al. (1999). The initial uptake of atmospheric CO₂ results in a δ¹³C isotopic change of +0.25‰. The release of isotopically depleted CO₂ from a terrestrial biomass source after 8 ka BP until the pre-industrial period yields a modelled δ¹³C isotopic change of −0.25‰, which is inconsistent with the δ¹³C isotope measurements in the ice cores. The δ¹³C isotope measurements from this ice core analysis shows no change after 8 ka BP. Elsig et al. (2009) propose that the most plausible source for the increase in Holocene atmospheric CO₂ concentration is the result of the carbon compensation mechanism enhanced by a smaller contribution from late-Holocene coral reef building.

The recent evolution of Holocene GHG concentrations can be compared with the structure of the evolution of the changes during previous glacial to interglacial transitions as a means of searching for a Holocene analogue (Berger and Loutre, 2003). Attempts have been made to correlate Northern Hemisphere insolation changes with the rise and fall of these well-mixed greenhouse gases during the previous interglacials (Broecker and Stocker, 2006; Ruddiman, 2003; Vavrus et al., 2008). Producing a valid synchronization between glacial/interglacial transitions at each time period makes the analysis difficult as each interglacial has a unique orbital signature that is not especially similar to the present interglacial.

The nature of the sequence of glacial/interglacial transitions that have occurred over the past million years has been subjected to detailed investigation through the analysis of deep sea sedimentary cores and ice cores and detailed comparisons with

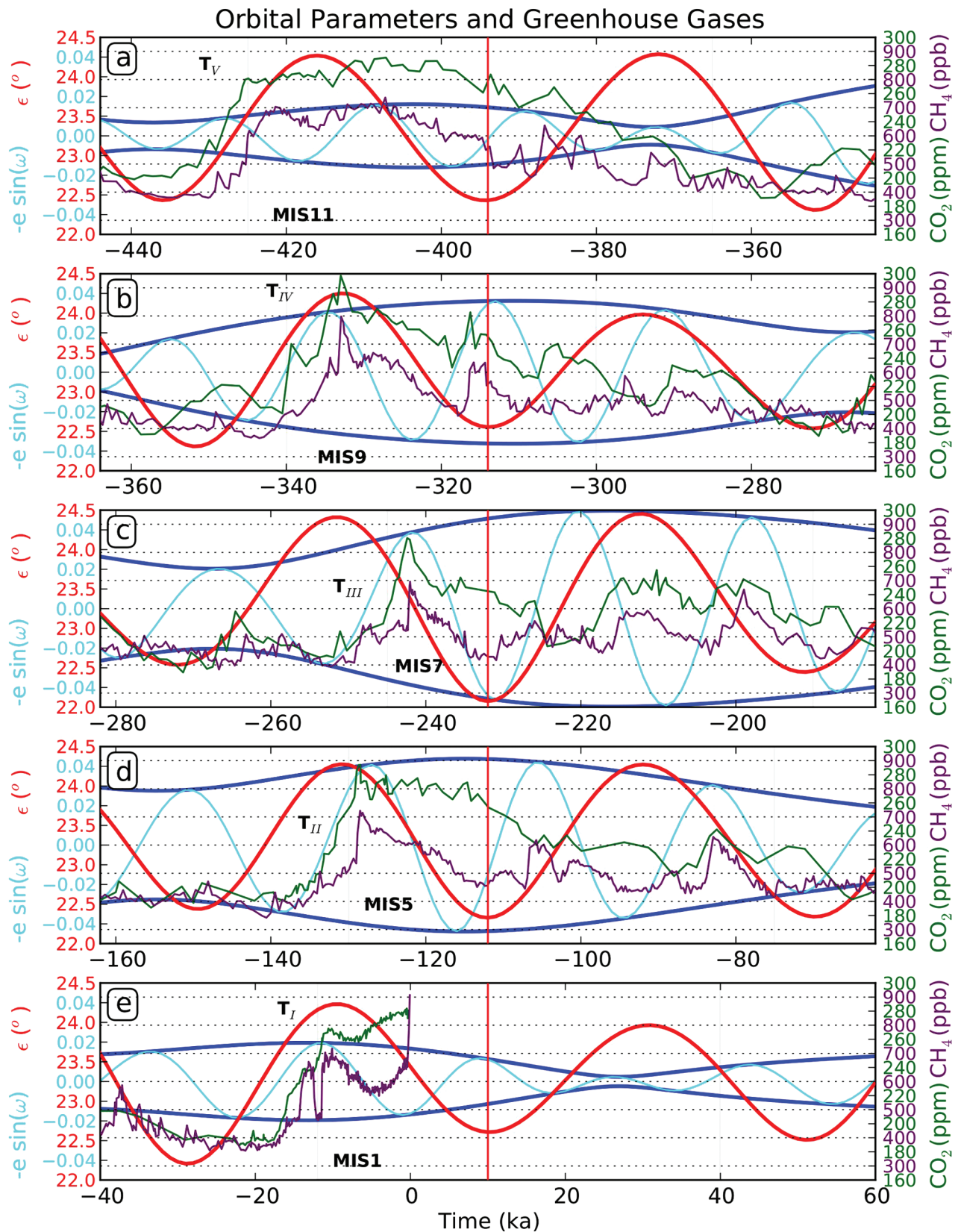


Figure I. Insolation and greenhouse gas concentration curves. Atmospheric carbon dioxide (green) and methane (purple) concentrations are from EPICA dome C. The eccentricity envelope (dark blue) and precessional parameter (cyan) are displayed with the obliquity (red) from Laskar (1990). The duration of each Marine Isotope Stage is indicated with a grey box and the phase locking of the obliquity minima in each stage are indicated with red vertical lines

insolation calculations (e.g. Hays et al., 1976). Here we assume a priori that the primary driver into a new glaciation period involves a complex interplay between eccentricity modulated precession

and obliquity, with obliquity being the dominant factor in driving high latitude land ice accumulation when eccentricity is low (Vettoretti and Peltier, 2004). Equally important for glacial

inception is the meridional insolation gradient and its influence on the meridional temperature gradient which is dominated by obliquity in summer (e.g. Berger, 1978; Davis and Brewer, 2009; Johnson, 1991; Raymo and Nisancioglu, 2003; Young and Bradley, 1984). New ice cores from Antarctica Dome C (EPICA Community Members, 2004) have provided detailed records of the last 800 000 years of CO₂ and CH₄ concentrations throughout the Quaternary (Loulergue et al., 2008; Lüthi et al., 2008). Here we superimpose upon variations in GHG concentration curves, the orbital parameters (Laskar, 1990) of eccentricity-precession ($-e \cdot \sin(w)$) and obliquity (e) (Figure 1). This analysis of the five isotope stages is presented so as to phase lock the obliquity minimum following the termination sequence of each marine isotope stage. These minima in obliquity occur at 394.0 ka, 314.0 ka, 232.0 ka and 112.0 ka before present (BP), and also at 10.0 ka after present (AP) in Figure 1(a)–(e), respectively.

This presentation contrasts five different glacial terminations with the oldest (MIS 11) starting with Termination five (T_v) at approximately 430 ka BP. The deuterium/hydrogen ratio in ice in the EPICA Dome C record indicates that the interglacials in the older part of the record were on average colder by more than 3°C (EPICA Community Members, 2004). The ice core records indicate that the interglacials before MIS 11 were characterized by atmospheric CO₂ and CH₄ concentrations that were much lower than after MIS 11 (Siegenthaler et al., 2005; Spahni et al., 2005). Thus there is a significant amount of interglacial diversity between the oldest four interglacials and the youngest five interglacials from the past 800 000 years (e.g. Tzedakis et al., 2009).

MIS 11 is often used as an analogue for the current Holocene interglacial as there are a number of similarities in the mean state of climate between the beginning of MIS 11 and the currently elapsed segment of the present interglacial (Loutre and Berger, 2003; McManus et al., 2003). There is, however, a significant discrepancy between the orbital signature of MIS 11 and the present interglacial. In particular, as Ruddiman (2007) has noted, the start of MIS 11 is characterized by a precession minimum and an obliquity maximum. In contrast, the early Holocene is characterized by a precession maximum at approximately 11 000 years ago, which is in phase with the obliquity maximum. In addition we note that there is the complicating factor that the eccentricity-precession envelope is in an increasing trend during the start of the MIS 11 interglacial while it is in a decreasing trend during the start of the most recent deglaciation. Therefore precession becomes more important going into the interglacial during MIS 11 relative to the present interglacial. In this current issue, Crucifix (2011) also stresses the lack of astronomical and insolation analogues for the modern Holocene. In particular, the study points out important caveats in the use of insolation analogues to predict climate change. Specifically this includes the idea of the importance of the particular climate state or the level of glaciation that precedes the glacial inception. Indeed most model simulations, including this study, evolve from the same initial conditions.

The increases in CO₂ and CH₄ that are clearly evident between 7000 years ago and present coincide with both a decreasing trend in precession forcing and a decreasing trend in obliquity. Ruddiman (2007) bases his early anthropogenic hypothesis on these observed changes in GHGs. Although a similar but somewhat less pronounced variation in atmospheric GHG concentrations is observed in the EPICA record between –415 ka and –405 ka, MIS 11 precession is out of phase with that of the modern configuration (Tzedakis et al., 2009). Further complicating this analysis is the

fact that this time period is deep in the record where measurement and dating error is much larger than in the earlier segment of the record (Dreyfus et al., 2007). Nevertheless this high quality record provides accurate absolute ages with a maximum uncertainty of 6 kyr throughout the entire 800 kyr record (Parrenin et al., 2007).

In the remaining sections of this paper we will further address the early anthropogenic hypothesis by examining the possibility of glacial inception during the modern pre-industrial era with a suite of modelling simulations that investigate the sensitivity of glacial inception to variations in GHG concentrations. We also investigate the relative roles of insolation and GHG forcing and the impact of ocean circulation on this process. In the next section we describe the model and experimental design, which is followed by an analysis of the results in the subsequent section. Conclusions are offered in the final section of the paper.

Model description and experimental design

The model to be employed in this study is the National Center for Atmospheric Research Community Climate Model Version 3 (NCAR CCSM3). The model is run in fully coupled mode, with atmosphere (CAM3), land (CLM3), ocean (POP) and sea-ice components (CSIM5). The atmosphere is resolved at a resolution of T42 (approximately $2.8^\circ \times 2.8^\circ$), with 26 levels in the vertical (Collins et al., 2006a, b). The land surface (Dickinson et al., 2006) is at the same resolution as the atmosphere and contains a detailed treatment of the hydrological cycle. The ocean component of the model is represented on a orthogonal grid of varying resolution of approximately $1^\circ \times 1^\circ$ (higher resolution in the tropics and lower resolution at the poles) with the poles centered on Antarctica and Greenland, with 40 levels in the vertical (Smith and Gent, 2004). The sea-ice module operates on the same grid as the ocean model and includes full thermodynamic and dynamic sea-ice calculations (Holland et al., 2006). Further details of the model control climate and land surface parameterizations that influence the evolution of the cryosphere are described below. For details regarding the fully coupled CCSM3 see Collins et al. (2006a, b).

The land surface model (CLM3) has a spatial land surface heterogeneity that is represented as a nested subgrid hierarchy of grid cells composed of land unit types (e.g. glacier, vegetated land, etc.), snow/soil columns, and plant functional types (PFTs). The snow/soil column can have up to ten soil layers and up to five snow layers depending on snow depth. There is no dynamic vegetation in this component of the model, and thus there is no feedback between changes in land surface characteristics and changes in snow cover and temperature. PFTs can coexist with snow cover within a grid cell, but exposed stem and leaf area can be considered completely snow covered if there is sufficient snow cover in a grid cell. The surface albedo is a function of the PFT canopy radiative transfer and the fraction of ground covered with snow, which is in turn a function of the snow depth. The net radiation at the surface is a balance between the net shortwave energy absorbed by the vegetation and ground and the net longwave emitted by the surface. Also included is the transfer of momentum and sensible and latent heat between the surface and atmosphere. The model parameterizes surface hydrology through interception, throughfall, canopy drip, snow accumulation and melt, water transfer between snow layers, infiltration, surface runoff, subsurface drainage, and redistribution within the soil column to

Table 1. A set of two control experiments and six glacial inception experiments, each with changes in atmospheric greenhouse gas concentration and orbital configuration

Simulation	CO ₂ concentration	CH ₄ concentration	N ₂ O concentration	Insolation
Modern control	355 ppmv	1714 ppbv	311 ppbv	Modern
Pre-industrial control	280 ppmv	700 ppbv	265 ppbv	Modern
Pre-industrial, high GHG	260 ppmv	500 ppbv	260 ppbv	Modern
Pre-industrial, medium GHG	250 ppmv	450 ppbv	250 ppbv	Modern
Pre-industrial, low GHG	240 ppmv	400 ppbv	240 ppbv	Modern
MIS5e/5d, high GHG	260 ppmv	500 ppbv	260 ppbv	116 ka BP
MIS5e/5d, medium GHG	250 ppmv	450 ppbv	250 ppbv	116 ka BP
MIS5e/5d, low GHG	240 ppmv	400 ppbv	240 ppbv	116 ka BP
10 ka AP, high GHG	260 ppmv	500 ppbv	260 ppbv	10 ka AP
51 ka AP, high GHG	260 ppmv	500 ppbv	260 ppbv	51 ka AP

simulate changes in canopy water, snow water, soil water and soil ice. All surfaces are constrained to have a snow water equivalent of less than 1000 kg/m². For fully snow-capped surfaces other than glaciers and wetlands, all solid and liquid precipitation reaching the ground in solid or liquid form, is explicitly assigned to runoff. This has particularly serious implications for formation of ice sheets in glacially sensitive regions. Since there is no fully coupled land ice/glacier model employed in this study, the extra runoff that is sent to the ocean when the model is at the limiting value of the maximum snow depth, there is no way to build the thickness of an ice sheet which could then flow to lower latitudes (Tarasov and Peltier, 1999). For further details of CLM3 see Oleson et al. (2004).

There are two control simulations employed as basis for the analysis to be presented in this study, one modern and one pre-industrial, that are used to compare both the modern climate against observations and to compare pre-industrial perennial snow accumulation against a set of experiments. The control simulations have been run to equilibrium for more than one millennium. In addition, we have conducted a series of six model experiments, each of which has been equilibrated and run for 700 years of simulation starting from the same initial state as the pre-industrial control (Table 1). The experiments include changes in GHG concentrations from what we term high (CO₂=260 ppmv), medium (CO₂=250 ppmv) and low (CO₂=240 ppmv), along with changes in insolation (modern and 116 ka BP) to form a set of six variations in boundary conditions. In addition to this, two future analyses for 10 ka AP and 51 ka AP were run for 400 years to assess the sensitivity to glacial inception at these future times. These future experiments were performed with high GHG forcing (CO₂=260 ppmv). For the boundary conditions used in each of the control and perturbation experiments, see Table 1.

More than 1000 years of the pre-industrial control simulation (CO₂=280 ppmv) have been run to investigate the nature of the variability of both the Atlantic Meridional Overturning Circulation (AMOC) and model surface temperature. In particular, we note a clear connection between the AMOC and the high latitude land surface temperature in the model (Figure 2). The AMOC maximum in the model undergoes a steady decline in strength over the first 500 years of simulation until a fairly stable regime of AMOC variability is achieved. This highlights the need for significantly lengthy runs in modelling the state of past climates in which model boundary conditions are significantly altered (Peltier and Solheim, 2004). Here the AMOC maximum obtains a value of approximately 18 Sv with significant annual to decadal

variability as demonstrated by the changes in the annual and the 20 yr running mean. It is not surprising to see the strong correlation between the decrease of the AMOC maximum and the land surface temperature in the Arctic between 60° and 70° N latitude. The decadal variability in high latitude surface temperature and AMOC maximum are almost precisely in phase demonstrating a connection between ocean dynamics and high latitude climate. This may be expected to impact the high latitude snow accumulation in each of the glacial inception experiments and illustrates the need to have a stable control climate along with a clear understanding of the nature of the decadal variations in the control climate. This will be discussed further in the following results section.

Model results

The factors influencing glacial inception in a coupled climate model are numerous and are strongly related to the control climate that is itself influenced by topography, model resolution, model sensitivity, snow parameterizations and climate system feedbacks. The most important factors for producing permanent snow cover at high northern latitudes during periods of low Northern Hemisphere summer insolation and reduced GHG concentrations are the surface temperature and precipitation amount. The interannual and decadal variability of a coupled model, and the teleconnections which are expressed in these fluctuations may also play a role causing the system to cross the critical threshold beyond which perennial snow cover begins.

The modern control climate in CCSM3 has been thoroughly documented in the literature. The main shortcoming in the model, which is further documented here involves high latitude summertime temperatures which are too cold by 2–6°C in some high latitude land areas (Dickinson et al., 2006). In particular, a comparison of Arctic August NCEP reanalysis surface temperature (Kistler et al., 2001) and the anomaly of modelled Arctic August surface temperature (i.e. the difference between observed and model predicted temperature) reveals a general cold bias over much of the high latitude land areas in the Northern Hemisphere (Figure 3(a, b)). In particular there are significant cold biases in eastern Siberia, Western Canada and Alaska of approximately 6–8°. There is also, however, a slight warm bias in the Canadian Arctic Archipelago of approximately 2°.

A comparison of Arctic August observed snow cover (NOAA/OAR/ESRL PSD, available at: <http://www.esrl.noaa.gov/psd/>) and modelled Arctic August snow cover reveal a lack of snow

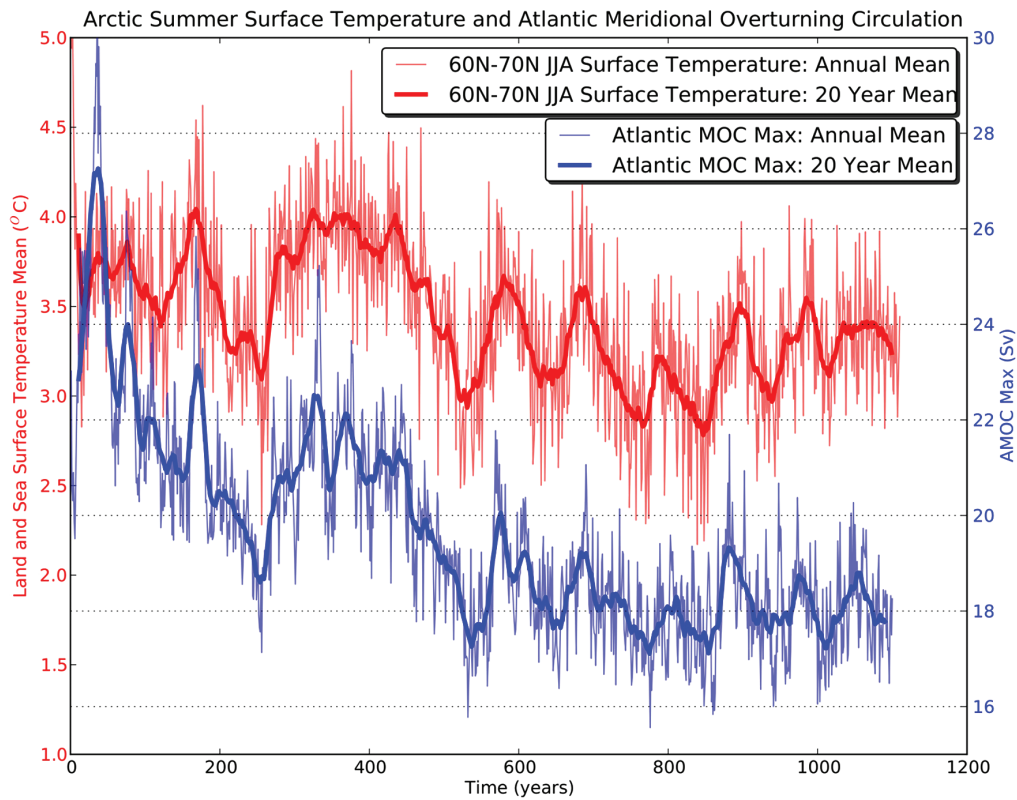


Figure 2. The pre-industrial control simulation Atlantic Meridional Overturning Circulation maximum (blue) and Arctic surface temperatures (ocean and land) through the spin-up to equilibrium

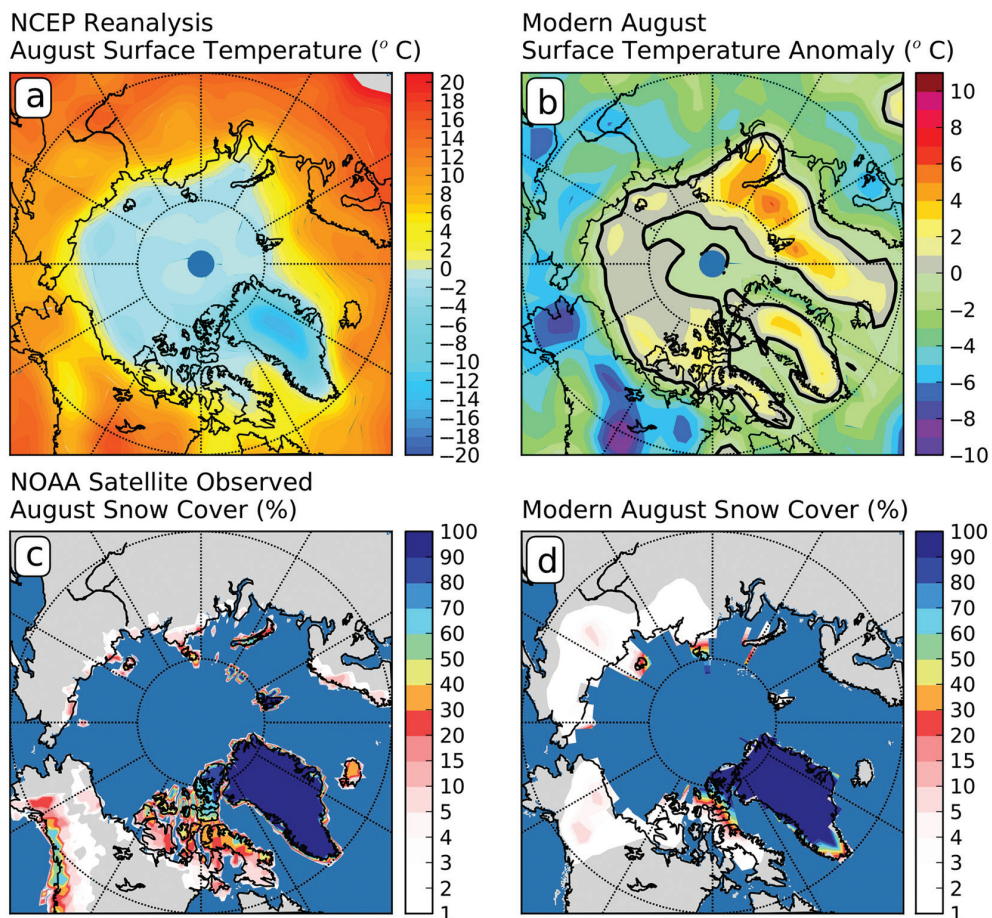


Figure 3. (a) The observed surface temperature ($^{\circ}\text{C}$) from the NCEP reanalysis and (b) the temperature anomaly between the modern simulation and the observed. The zero line is highlighted with a thick contour. (c) The fractional snow cover (%) observed from NOAA satellite observations and (d) the simulated fractional snow cover in the model

cover in the Canadian Arctic Archipelago and a surplus of low fractional snow cover over Alaska and Eastern Siberia (Figure 3(c) and (d), respectively). These regions with a small anomalous snow cover generally correspond with regions with negative temperature anomalies. This has implications for glacially sensitive regions important in glacial inception as has been demonstrated in previous studies (e.g. Vettoretti and Peltier, 2003a). Other model biases include excessive precipitation in the boreal extratropics throughout the year (Hack et al., 2006) and excessively deep snow cover in Northern Hemisphere regions (Dickinson et al., 2006). Temperatures in winter suffer from a slight warm bias in the model as a result of errors in the cloud distribution and low snow albedos (Collins et al., 2006b; Oleson et al., 2004; Vavrus and Waliser, 2008). The low snow albedos may also be a mitigating factor in the glacial inception process.

Another important model bias occurs in the simulation of sea ice in the model. The simulation of excessive sea ice is expected to impact the Arctic hydrological cycle and as a result distribution of perennial snow cover in the model experiments. In a study investigating the performance of the CCSM3 sea-ice model to the parameterization of ice thickness distribution, Holland et al. (2006) describe some of the shortcomings of the sea-ice component of the model. In particular, in the Northern Hemisphere, there are some notable biases including relatively extensive winter ice cover in the Labrador Sea and North Pacific, too little ice cover in the Barents Sea, and an unrealistic Arctic ice thickness pattern, and relatively thick ice along the Siberian coast and relatively thin ice along the Canadian Arctic Archipelago. This results correlate well with the temperature anomalies in Figure 3(b), and suggest that the fractional snow cover anomalies in Alaska and

Eastern Siberia noted in Figure 3(d) may result from excessive sea ice in this region.

A 20 yr average perennial snow cover anomaly is displayed in Figure 4 for the model experiments. The set of six experiments reveals differences between the pre-industrial control climate and the climates obtained when both GHG concentrations and insolation are varied. The dominant increases in perennial snow cover, relative to the pre-industrial control run, are a result of reductions in insolation to those characteristic of 116 ka BP (Figure 4(d)). The insolation changes in this set of experiments (Figure 4(d)–(f)) provide the strongest forcing for glacial inception. In the experiments that use modern insolation (Figure 4(a)–(c)), the anomalies in perennial snow cover due to the reductions in GHG concentrations are slightly smaller than the anomalies in the 116 ka BP insolation experiments. In fact, the GHG reductions in the 116 ka BP insolation experiments increase snow cover over Western Alaska, Central Siberia, and Northern Canada. The increases in perennial snow cover that occur over Alaska and Northeastern Siberia are areas that are known to have been ice free during the most recent glacial cycle (Gualtieri et al., 2003). The major changes in perennial snow cover under reductions in GHG concentration occur south of the Canadian Arctic Archipelago and most significantly in the experiments that are forced with the 116 ka BP insolation regime (Figure 4(d)–(f)). The distribution of the changes in perennial snow cover is generally correlated with the errors in the control model in August temperature and fractional snow cover that is explicitly documented in Figure 3. In particular, the changes in eastern Siberia and Alaska appear to be influenced by the discrepancies between the modern control climate and the observations (e.g. Vettoretti et al., 2003a).

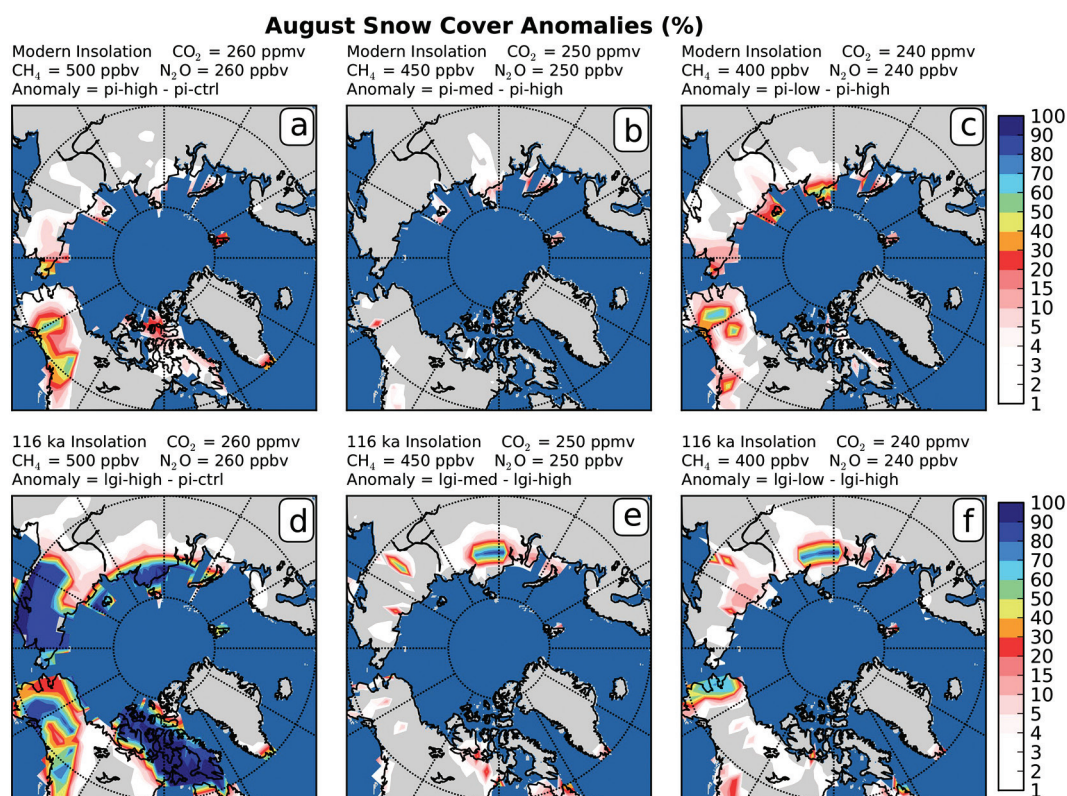


Figure 4. The fractional August snow cover anomalies (%) in each of the pre-industrial insolation simulations ((a)–(c)) and the 116 ka BP insolation simulations ((d)–(f)) with varying degrees of atmospheric greenhouse gas concentrations. (a),(d) high GHG concentrations; (b),(e) medium GHG concentrations; and (c),(f) low GHG concentrations

The parameterizations discussed previously in connection with the experimental design are expected to have a significant influence on the distribution of perennial snow cover in these experiments. In particular, the limitations on the accumulation of snowfall beyond 1 m of equivalent water depth, triggers a spurious runoff in the component of the hydrological cycle that is critical in building an ice sheet that would then flow under the influence of gravity towards lower latitudes. The incorporation of an ice-sheet model fully coupled to the atmosphere–ocean–land surface climate model will clearly be necessary to fully validate the conclusions of this study discussed below.

The variations in GHG concentration and insolation in each of the simulations we have discussed provide a means whereby the sensitivity of this model to initiating perennial snow cover at high latitudes may be assessed. The response of the amplitude of the AMOC maximum to these changes in boundary conditions also provides an additional means of assessing the impact of model internal variability on the glacial inception process. What is particularly important in the present study is to separate the relative importance of each factor in contributing to the inception process. In Figure 5 we illustrate the relative role that each of these factors plays in the set of sensitivity experiments by displaying the variations of global average surface temperature, Arctic summer land

surface temperature, Arctic snowfall over land, and the response of the amplitude of the AMOC over the last 200 years of each statistically equilibrated simulation. Each of the annually averaged 200 yr time series are displayed with a 20 yr running mean to better highlight the interannual and decadal variations occurring in each of the experiments.

On an annually and globally averaged basis, changes in insolation would have a negligible effect if it were not for the dominance of land masses in the Northern Hemisphere (Figure 5(a)). For example, at 116 ka BP the reduced summer insolation at mid to high northern latitudes is compensated by increased winter insolation in the Southern Hemisphere tropics and mid-latitudes. In fact, the changes in global average temperature in these experiments are dominated by reductions in GHG concentrations. The temperature ranges between 12°C and 13°C from the low GHG experiments to the high GHG experiments, respectively, with insolation playing a rather minor role.

If we instead focus on the annual and decadal variability of the high latitude Arctic summer land surface temperatures (Figure 5(b)), we see that the changes in temperature are completely determined by the insolation regime characteristic of the experiment. The changes in land surface temperature in the GHG experiments with the 116 ka BP insolation regime are up to 3°C colder than in the

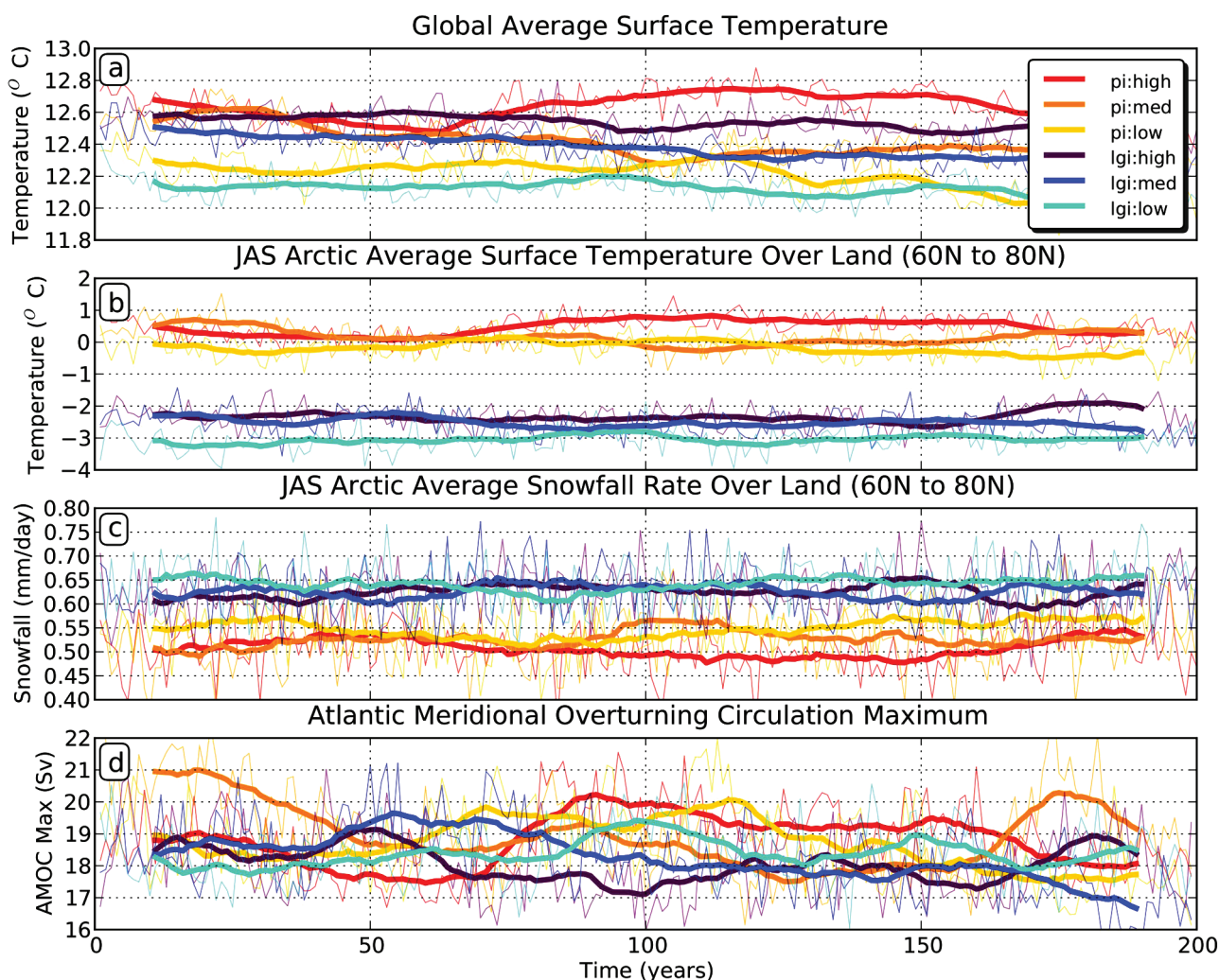


Figure 5. (a) The global and annual surface temperature (°C) in each of the six experiments during the last 200 years of the equilibrated climate (years 500–700). (b) The July–August–September Arctic land surface temperature (°C), (c) July–August–September Arctic snowfall rate (mm/day) over land, and (d) Annual Mean Atlantic Meridional Overturning Circulation maximum (Sv) are also displayed the same as in (a). The thick lines indicate the 20 yr running means

pre-industrial experiments with varying GHG concentrations. The insolation changes bring the climate from a zero melting point regime to well below freezing. This has significant implications for the role of GHG concentrations in creating conditions that are favourable to glacial inception during the latter part of the Holocene. If the high latitude model sensitivity to GHG concentrations in the model is correct, then variations in CO₂ concentrations between 240 and 280 ppmv are expected to have approximately 30% of the forcing (~1°C) relative to insolation on creating conditions that are favourable for high latitude perennial snow accumulation.

Since the snow cover parameterization in the land surface model has some significant glaciological implications in the formation of perennial ice sheets and glaciers, we instead analyse the flux of solid precipitation to the land surface in each of the experiments (Figure 5(c)). The snowfall rate is much more variable than that of the surface temperature over high latitude land areas. The 20 yr running mean provides a more robust indication of the decadal variations in snowfall rate in these high latitude areas. The most significant change in each of the experiments is the increase in the rate of snowfall with decreases in summer insolation characteristic of 116 ka BP. The impact of reductions in GHG concentrations appear to play a secondary role in the equilibrated perennial snow cover simulations. In particular, no significant change is seen in the snowfall rate in the 116 ka BP insolation experiments with variations in GHG concentration. In the pre-industrial insolation regime, the GHG concentration variations appear to have some influence on snowfall rate in the latter 100 yr segment of the 200 years of equilibrated climate.

Changes in AMOC strength may be related to changes in the phase of the Arctic Oscillation (Thompson and Wallace, 1998) which governs much of the interannual variability in the Arctic through ocean–atmosphere coupling (Lohmann et al., 2009). Recently, in a long coupled model simulation of the pre-industrial climate using CCSM3, the Atlantic Multidecadal Oscillation (AMO) that is associated with AMOC strength was found to exhibit a 60 yr cycle in variability (d’Orgeville and Peltier, 2009). However, changes in sea ice were shown not to be sufficient to explain changes in the AMOC variability. The AMOC amplitude (Figure 5(d)) is characterized by interannual and decadal variability varying between 17 and 20 Sv in all of the simulations. It is possible that these changes in AMOC strength impact the changes observed in the globally averaged and regionally averaged surface temperatures (Figure 5(a) and (b)). This correlation between high latitude surface temperature and AMOC that was clearly visible in Figure 2 is not so apparent in each of the perennial snow cover experiments. Thus we have employed a regression analysis in what is to follow.

A regression analysis between the 20 yr running mean Arctic summer surface temperature, Arctic summer snowfall rate and AMOC strength are displayed in Figure 6. The regression between surface temperature and snowfall rate indicates only a slight sensitivity of the model to the changes in the GHG concentration in both the pre-industrial experiments and the 116 ka BP experiments. The R^2 correlation coefficient indicates that there is a higher degree of correlation between surface temperature and snowfall in the pre-industrial CO₂ sensitivity experiments. The significant changes in snowfall rate occur in the 116 ka BP experiments as described in Figure 5. In each pre-industrial experiment, the correlation between surface temperature and AMOC strength displays roughly the same degree of sensitivity to CO₂ as in

Figure 6(a). While the Arctic surface temperature changes in the set of six experiments, the AMOC appears relatively insensitive to both insolation forcing and CO₂ forcing. In a previous study, Khodri et al. (2001) also find that the AMOC maximum does not change significantly between their 115 ka BP simulation and their control simulation. In the regression analysis between snowfall and AMOC strength the correlations are evident in the pre-industrial experiments but completely break down in the 116 ka BP experiments. In general, the regression analysis indicates that the AMOC strength appears relatively insensitive (2–3 Sv) to changes in both CO₂ and insolation forcing. Thus, insolation and CO₂ forcing appear to have more of an impact on the snowfall rate at high latitudes rather than do changes in internal ocean variability.

The next glacial cycle

The nature of the ongoing Holocene/Anthropocene transition has provided much stimulus for discussion as to if or when a next transition into glacial conditions will occur. One modelling study, which employed varying amounts of atmospheric GHG concentrations, suggests that the next glacial cycle will not begin for another 50 000 years (Berger and Loutre, 2002). There is also interest in the extent to which human influence might play a role in any such event (Crucifix and Berger, 2006). The current analysis in Figure 1 may be further employed to investigate the point at which GHG concentrations respond to decreases in insolation. In MIS 5, 7 and 9, precession is clearly a significant factor in reducing GHG concentrations a half precessional cycle after the end of the termination event which marks the beginning of each of these marine isotope stages. The high value of orbital eccentricity exerts a strong control on the summer insolation minimum during each of these three stages (Figure 1(b)–(d)). The orbital signatures of MIS 11 and MIS 1 have much greater similarity that extends well into the interglacial between 380 and 360 ka before present and 20 and 40 ka into the future. Both epochs are characterized by near zero eccentricity and maximum obliquity. Despite this period of coincident orbital configuration with precession exerting a smaller influence on the radiative forcing regime, the Earth is well into a glacial state at 370 ka BP. The largest initial rate of decrease in GHG concentration during MIS 11 occurs during the obliquity minimum at 394 ka (Figure 1(a)). This is a period when obliquity and precession have reached their respective minima in phase.

The best modern analogue for the 394 ka BP obliquity minimum would be 10 000 years into the future, when obliquity will reach a minimum that is preceded by an increasing trend in precession. The different phase relationship between precession in these two periods would suggest that a direct comparison between MIS 11 and the current interglacial would be inexact. However, a closer investigation of the insolation incident at the top of the atmosphere during these two obliquity minima reveal that the two periods have strikingly similar insolation forcing (Figure 7(a) and (b)). The period at 394 ka BP is a period when the atmospheric GHG concentration is falling rapidly and land ice volume is increasing sharply (Figure 1(a); Kariya et al., 2010) from a level similar to that characteristic of the modern Holocene (Bowen, 2010). Earlier modelling studies (Berger and Loutre, 2002) using a zonally averaged quasi-geostrophic atmospheric model coupled to a simple mixed-layer ocean and ice-sheet model (Gallée et al., 1991) suggested that the next glacial cycle will not commence for another 50 000 years. The insolation anomaly between 51 ka BP

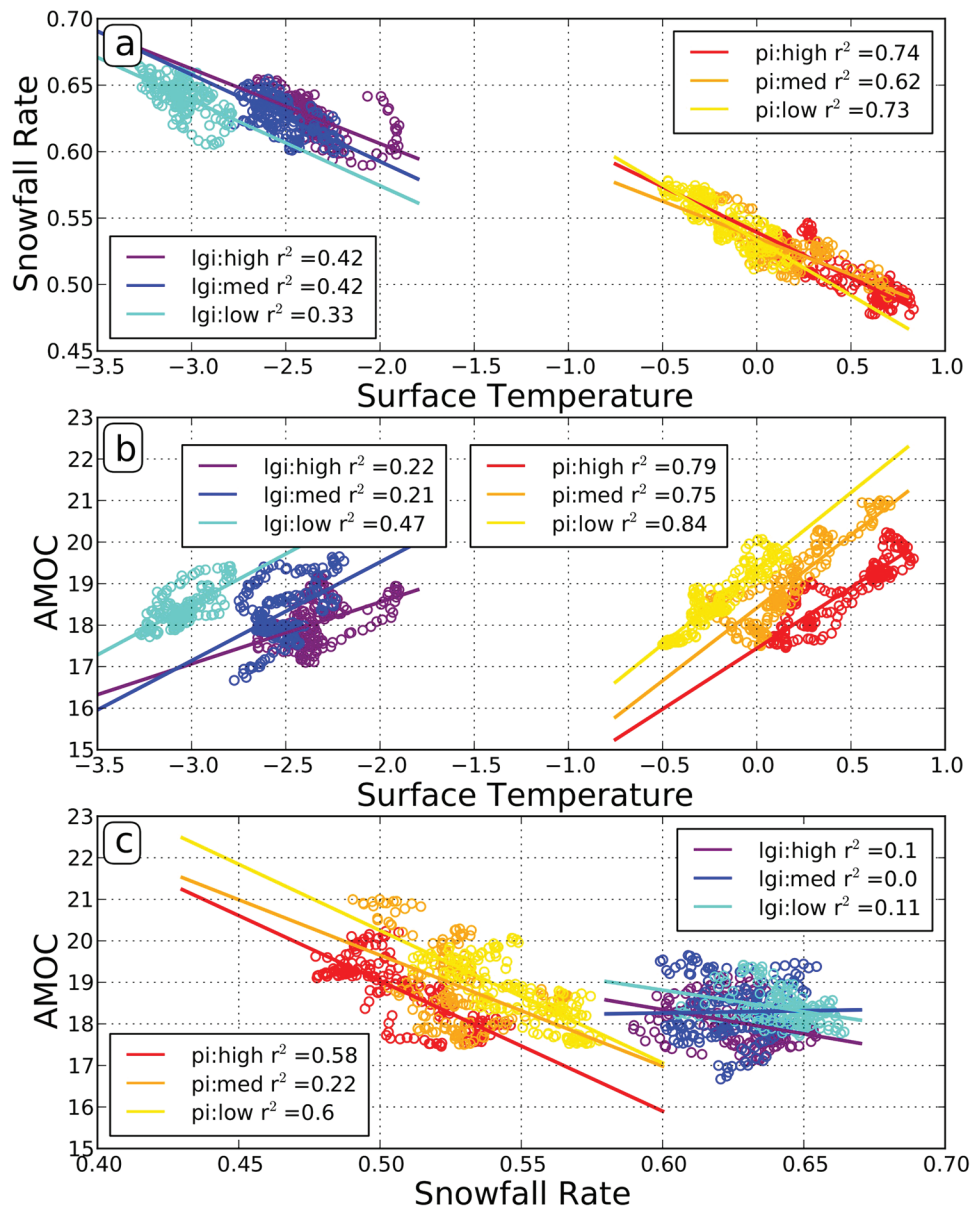


Figure 6. The regression between 20 yr running mean surface temperature, snowfall rate and AMOC maximum in each of the six perennial snow cover experiments during the last 200 years of the equilibrated climate. (a) Surface temperature versus snowfall rate. (b) Surface temperature versus AMOC maximum. (c) Snowfall rate versus AMOC maximum

and modern (Figure 7(c)) is characteristically different from the 394 ka BP and 10 ka AP insolation anomalies. The 51 ka BP insolation anomaly has an Arctic spring insolation minimum while the 394 ka BP and 10 ka AP insolation have Arctic late summer insolation minima more consistent with the Milankovitch hypothesis of glacial initiation (Figure 7(c) and (d)). We propose an alternate scenario based upon the insolation radiative forcing presented in Figure 7, that the period approximately 10 000 years into the future would be seen as a period that is favourable for the full onset of the next glacial cycle.

This onset of the next glacial cycle is of course subject to the caveat that by that time the influence of postindustrial anthropogenic increases in GHG concentration would have been eliminated from the system. Archer et al. (2009) have provided an extensive discussion of the long-timescale absorption of atmospheric CO_2 by the Earth system over the next 10 000 years. In Figure 8 we present a CO_2 decay curve which is a schematic representation modelled after Eby et al. (2009). The decay curve for

a 2560 Gt impulse of carbon into the atmosphere, which represents half of the fossil fuel reserves available for consumption, does not follow a simple exponential curve because different chemical and physical processes operate at different timescales (Berner, 2004, 2006). The initial large drop in CO_2 concentration over the first few hundred years is due to the uptake and resulting acidification of the upper ocean. This occurs in conjunction with the uptake of CO_2 by the land-biosphere system. Over the timescale of 2–20 centuries the deep ocean circulation removes CO_2 from the upper ocean and allows for the re-absorption of additional CO_2 from the atmosphere. Over the following several thousand years, the remaining CO_2 in the atmosphere is taken up by pH-neutralization reactions with calcium carbonate (CaCO_3) dissolution from the sea floor and the CaO component of igneous rocks. The final long-timescale decay process involves calcium-magnesium silicate weathering of the surface of the continents. These processes are expected to return the atmospheric CO_2 concentrations back to pre-industrial levels but on a long 100 000 yr

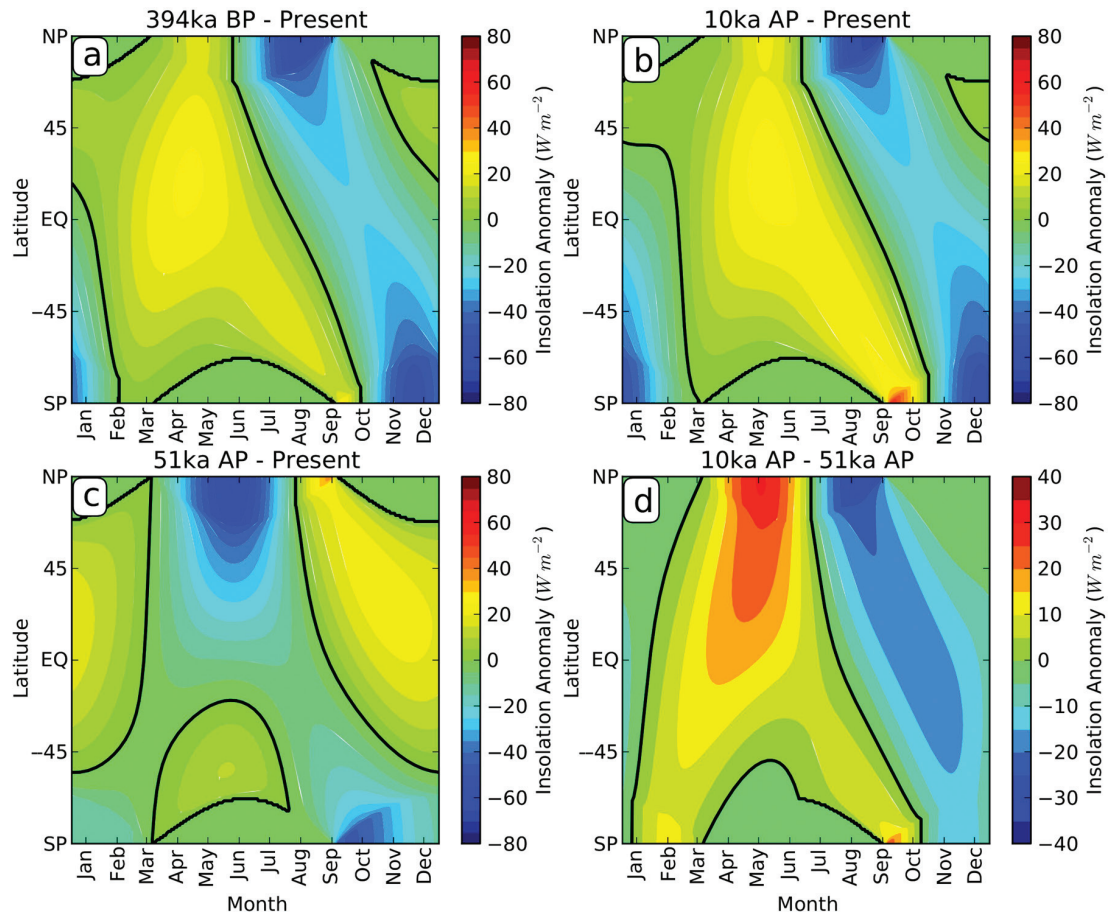


Figure 7. The insolation anomalies (W m^{-2}) at the top of the atmosphere between (a) 394 ka before present (BP) and modern, (b) 10 ka after present (AP) and modern, (c) 51 ka AP and modern, and (d) 10 ka AP and 51 ka AP. The zero line is highlighted with a thick contour. The insolation anomalies are calculated from the orbital parameter calculations of Berger (1978)

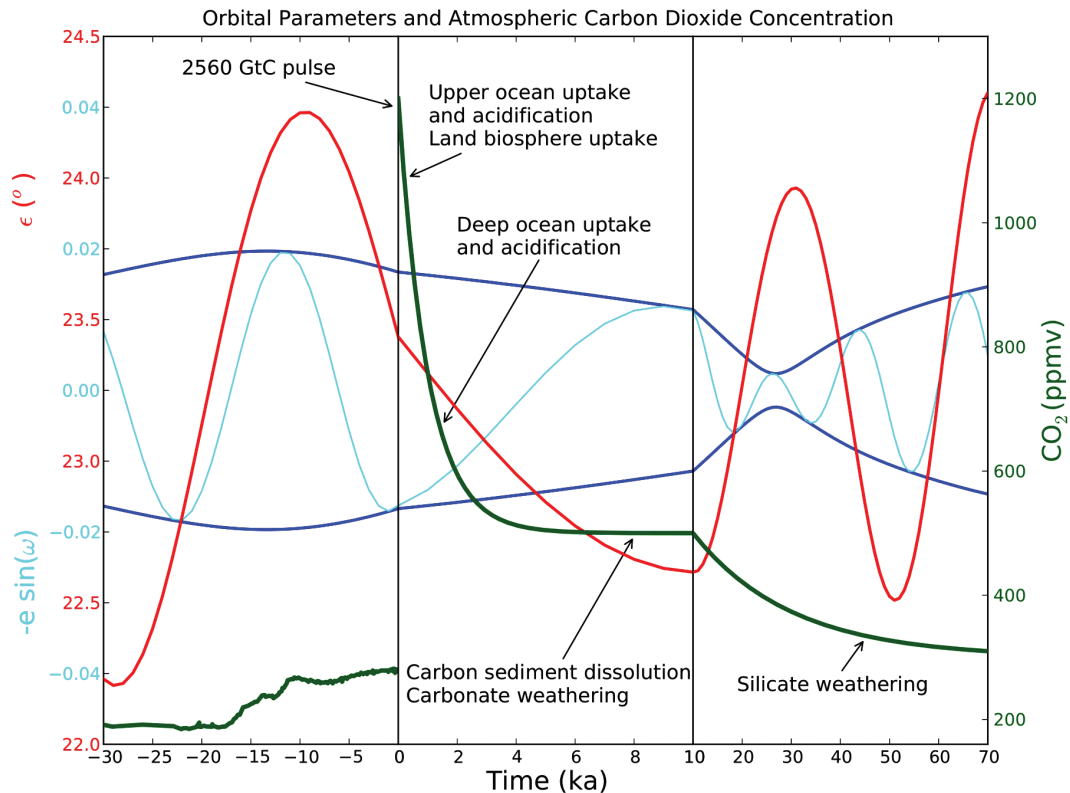


Figure 8. The long term evolution of CO_2 concentration in the atmosphere (green) after the input of a 2560 Gt pulse of carbon into the atmosphere. The CO_2 decay is modelled after Eby et al. (2009). The eccentricity envelope (dark blue) and precessional parameter (cyan) are displayed with the obliquity (red) as in Figure 1

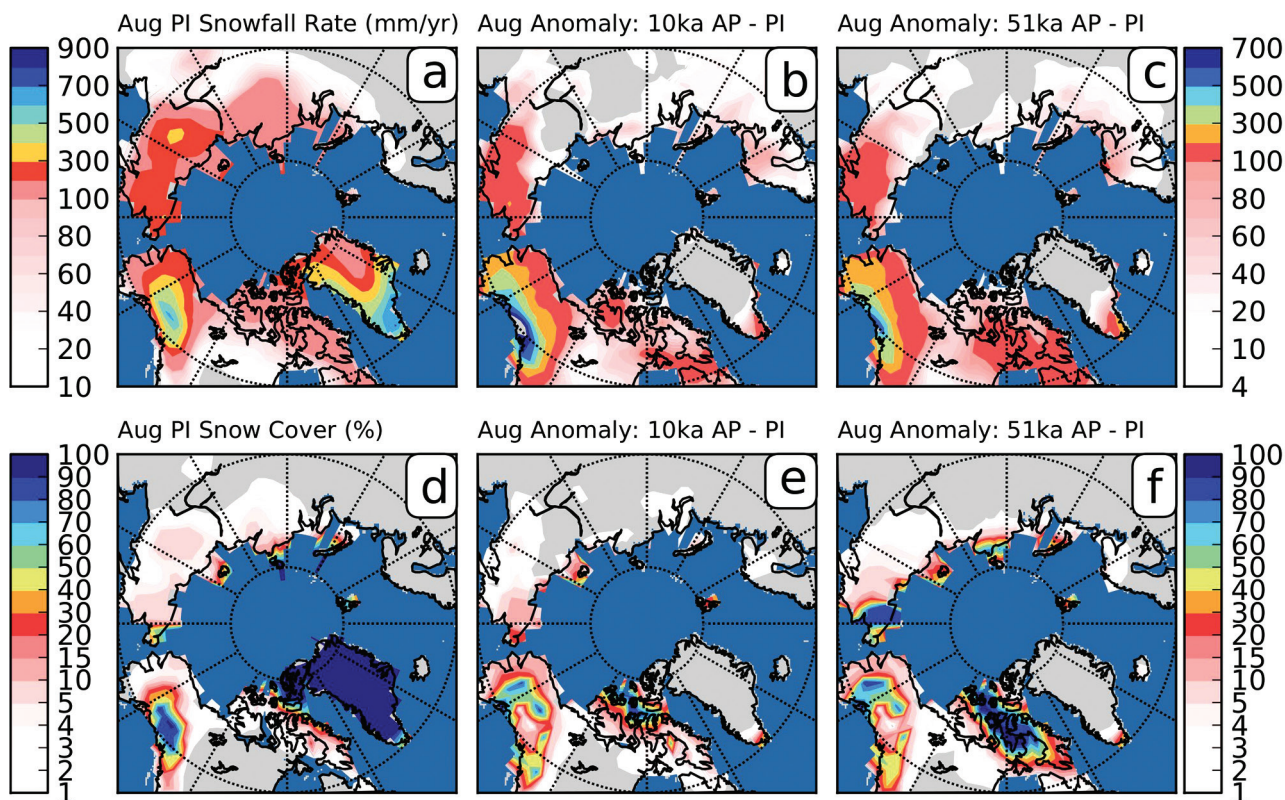


Figure 9. August snowfall rate (mm/yr) for (a) pre-industrial simulation with high GHG levels. Anomalies for (b) 10 ka AP (high GHG level) – pre-industrial (high GHG level) and (c) 51 ka AP (high GHG level) – pre-industrial (high GHG level). (d), (e) and (f) Same as in (a), (b) and (c) but for August snow cover fraction (%). The colour bar on the right represents the changes in the the anomalies ((b), (c), (e) and (f))

timescale (Figure 8). The model intercomparison described in Archer et al. (2009) suggests that 20–35% of the initial atmospheric CO_2 pulse remains in the atmosphere even after 10 000 years.

Eby et al. (2009) also makes the important point that the radiative forcing of CO_2 is non-linear and thus the radiative forcing will have a longer lifetime than the actual rate of removal of CO_2 from the atmosphere. With the obliquity reaching a minimum at 10 ka BP (Figure 8), the question of whether this period would be favourable to glacial inception is dependent on the magnitude of the CO_2 pulse released into the atmosphere during this century.

In a preliminary analysis to highlight the sensitivity of the model to glacial inception in the future we have run two additional simulations with high GHG levels ($\text{CO}_2=260$ ppmv) for 10 ka AP and 51 ka AP. The high GHG pre-industrial simulation snowfall rate (mm/yr) is displayed in Figure 9(a) along with the snow cover (%) in Figure 9(d). The snowfall rate and snow cover anomalies for the 10 ka AP and 51 ka AP experiments are displayed in Figure 9(b) and (c) and Figure 9(e) and (f), respectively. The changes in snow cover for the high GHG pre-industrial simulation (Figure 9(d)) are similar to the changes observed in the pre-industrial control ($\text{CO}_2=280$ ppmv; not shown). In fact the pre-industrial control experiment ($\text{CO}_2=280$ ppmv) and high GHG pre-industrial ($\text{CO}_2=260$ ppmv) shows permanent snow cover over Ellesmere Island and the St Elias Mountain Range. From this initial analysis we see that the 10 ka AP simulation displays increased snowfall and increased perennial snow cover in the Canadian Arctic Archipelago, Alaska and Eastern Siberia more so than the pre-industrial high GHG experiment. The 51 ka BP experiment also shows similar regional changes as in the 10 ka

AP experiment but of a stronger magnitude. While an in-depth analysis is beyond the scope of this study, these simulations indicate that the present interglacial will last for at most approximately 20 000 years in the absence of modern anthropogenic GHG forcing (Figure 8). This is contrary to an earlier study that suggests the start of the next interglacial to occur 50 000 years into the future (e.g. Berger and Loutre, 2002). The latter scenario would be the more likely, of course, if the anthropogenic impact on GHG levels remained high at 10 ka AP.

Conclusions

We have focused on a set of experiments, using a coupled atmosphere–ocean model of moderate resolution, to investigate the impact of both changes in GHG concentrations and insolation changes in order to better understand the influence that these boundary condition changes have on high latitude perennial snow cover in the model. The importance of internal decadal variability in the simulations was also addressed by examining the correlation between changes in the AMOC and changes in surface temperature and snow cover at high northern latitudes in each of the experiments. The purpose of this study was to address a number of long-standing issues regarding the relative role that GHG concentrations play as a determining factor in the growth of ice sheets in the Arctic under reduced northern summertime insolation conditions. The early anthropogenic hypothesis proposed by Ruddiman (2003) is predicated upon the notion that human modifications of the environment in the early to late Holocene may have contributed to the arrest of what would have otherwise been the onset of the next glacial cycle by increasing GHG concentrations in the atmosphere and thus warming the planet.

The excellent records of GHG concentrations from Antarctica, along with detailed calculations of insolation throughout the second half of the Quaternary allow us to draw analogues between the modern interglacial and the set of interglacials that have occurred in the past 800 000 years. MIS 11 and the modern interglacial, often used as analogues for one another, have a number of significant differences in orbital signature that make comparisons difficult. In particular, eccentricity-precession and obliquity are out of phase just after Termination five (MIS 11) and are in phase just after the last glacial termination that leads into the Holocene. We find that this basis of comparison is rather inconclusive as a means of addressing arguments for or against the early anthropogenic hypothesis. Instead we focus on a series of modelling studies with strong and weak insolation forcing and low and high GHG concentrations and including the internal variability characteristic of a coupled model.

The evolution of the AMOC is correlated with global and regional temperatures in the coupled model that we employ. Equilibrating the climate requires hundreds of simulation years to obtain a stable climate, that we have shown is characterized by large fluctuations in regional high latitude temperatures which correlate well with the AMOC maximum. The statistically equilibrated climate is also subject to a number of anomalies with respect to the modern observed climate. In particular, there are high latitude cold biases and anomalously high amounts of snow coverage in Northern Hemisphere summer. These biases are shown to manifest themselves in each of the glacial inception experiments presented in this study. In particular we find too much snow accumulation in the regions of northwestern North America and eastern Siberia. While we have not directly addressed the cause for this excessive snow accumulation, the errors in the sea-ice simulated in the CCSM3 (Holland et al., 2006) are a possible cause for this anomalous permanent snow cover. The land surface snow cover parameterization in the model also has a number of deficiencies in the physical simulation of permanent snow cover that includes limits on snow accumulation.

The set of six glacial inception simulations demonstrate that the impact of the 116 ka BP insolation regime is the strongest factor in determining the extent of perennial snow cover. The level of GHG concentrations (CO_2 between 240 and 260 ppmv) plays a secondary role in determining the extent of snow cover in both the pre-industrial era and at 116 ka BP. The changes in snowfall rate in the Arctic were shown to be highly correlated with surface temperature in these regions. The significant changes in snowfall rate were influenced to first order by insolation changes rather than the atmospheric GHG concentration. The decadal variability in Arctic summer surface temperature and snowfall appear to be correlated with AMOC strength but a regression analysis between these variables does not provide strong evidence for a relationship between AMOC strength and perennial snow cover changes. The AMOC strength appears relatively constant (to within 2–3 Sv) between the 116 ka BP experiments and the pre-industrial experiments. We are nevertheless unable to rule out the possibility that changes in internal variability of the climate system may play a significant role in the glacial inception process as longer and more detailed studies may be required (e.g. the melt back of Greenland during the end of the Eemian, when surface temperatures were 1–2°C warmer than present (Kaspar et al., 2005)).

The magnitude of the impact that early anthropogenic activity had on climate will require further analyses. This study, while not directly addressing the validity of the early anthropogenic

hypothesis, investigated the component of the hypothesis that suggested that early anthropogenic carbon emissions would have resulted in the suppression of the start of the next ice age well before the onset of the industrial revolution. The results of our analysis, which illustrate the impact of reductions in GHGs during the pre-industrial period (CO_2 from 240 to 280 ppmv), do not display any significant glacial inception in the Canadian Arctic Archipelago. This is contrary to the idea that changes in Holocene GHG concentrations of the magnitude suggested by Ruddiman (2007) would have been sufficient to eliminate the onset of perennial snow cover that would otherwise have occurred in the Holocene in the absence of anthropogenic forcing. Our analyses also suggest that insolation forcing is by far the most significant driver of the glacial inception process with GHG concentration playing a secondary role. Using an additional set of two simulations of the future (10 ka AP and 51 ka AP), we propose that the closest modern analogue for conditions favourable to glacial inception is less than 10 000 years into the future when Earth's obliquity achieves a local minimum and insolation is reduced in Northern Hemisphere late summer and fall at high latitudes. Our simulations, using mean interglacial GHG levels, indicate that the current interglacial will last for at most approximately 20 000 years. It will be interesting in future work to investigate the level of GHG concentrations that would have to be reached following injection of the CO_2 spike that humankind is currently adding to the system in order that a further glacial cycle may occur.

Acknowledgements

This work was supported through a multiyear grant awarded to the Polar Climate Stability Network that was funded by the Canadian Foundation for Climate and Atmospheric Sciences. We would like to thank Jerry McManus for insightful discussions that helped improve the manuscript. The computations on which this paper is based were performed on the IBM Power 6 supercomputer of the SciNet facility for High Performance Computation at the University of Toronto that is a component of the Compute Canada HPC platform.

References

- Archer D, Eby M, Brovkin V, Ridgwell A, Cao L, Mikolajewicz U et al. (2009) Atmospheric lifetime of fossil fuel carbon dioxide. *Annual Review of Earth and Planetary Sciences* 37: 117–134.
- Andrews JT and Mahaffy MAW (1976) Growth rate of the Laurentide ice sheet and sea level lowering (with emphasis on the 115,000 BP sea level lows). *Quaternary Research* 6: 167–183.
- Berger A (1978) Long term variations of daily insolation and Quaternary climatic changes. *Journal of the Atmospheric Sciences* 35: 2362–2367.
- Berger A and Loutre M-F (2002) Climate: An exceptionally long interglacial ahead? *Science* 297(5585): 1287–1288.
- Berger A and Loutre M-F (2003) Climate 400,000 years ago, a key to the future? In: Droxler AW et al. (eds) *Earth's Climate and Orbital Eccentricity: The Marine Isotope Stage 11 Question*. Geophysical Monograph Series, vol. 137. Washington DC: American Geophysical Union, 17–26.
- Berner RA (2004) *The Phanerozoic Carbon Cycle: CO_2 and O_2* . Oxford: Oxford University Press, 150 pp.
- Berner RA (2006) Inclusion of the weathering of volcanic rocks in the GEO-CARBUSUF model. *American Journal of Science* 306: 295–302.
- Bowen DQ (2010) Sea level approximately ~400,000 years ago (MIS11): Analogue for present and future sea-level. *Climate of the Past* 6: 19–29.

- Broecker WS and Stocker TL (2006) The Holocene CO₂ rise: Anthropogenic or natural? *EOS Transactions* 87: 27.
- Broecker WS, Clark E, McCorkle DC, Peng T-H, Hajdas I and Bonani G (1999) Evidence for the reduction in the carbonate ion content of the deep sea during the course of the Holocene. *Paleoceanography* 14: 744–752.
- Broecker WS, Lynch-Stieglitz J, Clark E, Hajdas I and Bonani G (2001) What caused the atmosphere's CO₂ content to rise during the last 8000 years? *Geochemistry Geophysics Geosystems* 2: 1062. doi:10.1029/2001GC000177.
- Calov R, Ganopolski A, Kubatzki C and Claussen M (2009) Mechanisms and time scales of glacial inception simulated with an Earth system model of intermediate complexity. *Climate of the Past* 5: 245–258.
- Calov R, Ganopolski A, Petoukhov V, Claussen M, Brovkin V and Kubatzki C (2005) Transient simulation of the last glacial inception. Part II: Sensitivity and feedback analysis. *Climate Dynamics* 24: 563–576.
- Claussen M, Berger A and Held H (2007) A survey of hypotheses for the 100-kyr cycle. *Developments in Quaternary Science* 7: 29–35.
- Claussen M, Brovkin V, Calov R, Ganopolski A and Kubatzki C (2005) Did humankind prevent a Holocene glaciation? *Climate Change* 69: 409–417.
- Collins WD, Bitz CM, Blackmon ML, Bonan GB, Bretherton CS, Carton JA et al. (2006a) The Community Climate System Model: CCSM3. *Journal of Climate* 19: 2122–2143.
- Collins WD, Rasch PJ, Boville BA, Hack JJ, McCaa JR, Williamson DL et al. (2006b) The formulation and atmospheric simulation of the Community Atmosphere Model Version 3 (CAM3). *Journal of Climate* 19: 2144–2161.
- Crucifix M (2011) How can a glacial inception be predicted? *The Holocene* (this issue). doi:10.1177/0959683610394883.
- Crucifix M and Berger AL (2006) How long will our interglacial be? *EOS Transactions* 87: 352–353.
- Crucifix M and Loutre MF (2002) Transient simulations over the last interglacial period (126–115 kyr BP): Feedback and forcing analysis. *Climate Dynamics* 19: 417–433.
- D'Orgeville M and Peltier WR (2009) Implications of both statistical equilibrium and global warming simulations with CCSM3. Part II: On the multidecadal variability in the North Atlantic basin. *Journal of Climate* 22: 5277–5297.
- Davis BAS and Brewer S (2009) Orbital forcing and role of the latitudinal insolation/temperature gradient. *Climate Dynamics* 32: 143–165.
- Deblonde G and Peltier WR (1991a) Simulations of continental ice-sheet growth over the last glacial–interglacial cycle: Experiments with a one-level seasonal energy balance model including realistic geography. *Journal of Geophysical Research* 96(D5): 9189–9215.
- Deblonde G and Peltier WR (1991b) A one-dimensional model of continental ice volume fluctuations through the Pleistocene: Implications for the origin of the mid-Pleistocene climate transition. *Journal of Climate* 4(3): 318–344.
- de Noblet NI, Prentice IC, Joussaume S, Texier D, Botta A and Axeltine A (1996) Possible role of atmosphere–biosphere interactions in triggering the last glaciation. *Geophysical Research Letters* 23: 3191–3194.
- Desprat S, Sanchez Goñi MF, Turon JL, McManus JF, Loutre MF, Duprat J et al. (2005) Is vegetation responsible for glacial inception during periods of muted insolation changes? *Quaternary Science Reviews* 24: 1361–1374.
- Dickinson RE, Oleson KW, Bonan G, Hoffman F, Thornton P, Versteinstein M et al. (2006) The Community Land Model and its climate statistics as a component of the Community Climate System Model. *Journal of Climate* 19: 2302–2324.
- Dreyfus GB, Parrenin F, Lemieux-Dudon B, Durand G, Masson-Delmotte V, Jouzel J et al. (2007) Anomalous flow below 2700 m in the EPICA Dome C ice core detected using δ¹⁸O of atmospheric oxygen measurements. *Climate of the Past* 3: 341–353.
- Eby M, Zickfeld K, Montenegro A, Archer D, Meissner KJ and Weaver AJ (2009) Lifetime of anthropogenic climate change: Millennial time-scales of potential CO₂ and surface temperature perturbations. *Journal of Climate* 22: 2501–2511.
- Elsig JJ, Schmitt D, Leuenberger R, Schneider M, Eyer M, Leuenberger F et al. (2009) Stable isotope constraints on Holocene carbon cycle changes from an Antarctic ice core. *Nature* 461: 507–510.
- EPICA Community Members (2004) Eight glacial cycles from an Antarctic ice core. *Nature* 429: 623–628.
- Gallée H, van Ypersele JP, Fichefet T, Tricot C and Berger A (1991) Simulation of the last glacial cycle by a coupled, sectorially averaged climate–ice sheet model. I. The climate model. *Journal of Geophysical Research* 96: 13 139–13 161.
- Gallimore RG and Kutzbach JE (1996) Role of orbitally induced changes in tundra area in the onset of glaciation. *Nature* 381: 503–505.
- Gualtieri L, Vartanyan S, Brigham-Grette J and Anderson P (2003) Pleistocene raised marine deposits on Wrangel Island, northeast Siberia and implications for the presence of an East Siberian ice sheet. *Quaternary Research* 59(3): 399–410.
- Hack JJ, Caron JA, Yeager SG, Oleson KW, Holland MM, Truesdale JE et al. (2006) Simulation of the global hydrological cycle in the CCSM Community Atmosphere Model Version 3 (CAM3): Mean features. *Journal of Climate* 19: 2199–2221.
- Hays JD, Imbrie J and Shackleton NJ (1976) Variations in the Earth's orbit: Pacemaker of the ice ages. *Science* 194: 1121–1132.
- Holland MM, Bitz CM, Hunke EC, Lipscomb WH and Schramm JL (2006) Influence of the sea ice thickness distribution on polar climate in CCSM3. *Journal of Climate* 19: 2398–2414.
- Johnson RG (1991) Major Northern Hemisphere deglaciation caused by a moisture deficit 140 ka. *Geology* 19: 686–689.
- Kageyama M, Charbit S, Ritz C, Khodri M and Ramstein G (2004) Quantifying ice-sheet feedbacks during the last glacial inception. *Geophysical Research Letters* 31: L24203. doi:10.1029/2004GL021339.
- Kariya CK, Hyodo M, Tanigawa K and Sato H (2010) Sea-level variation during MIS 11 constrained by stepwise Osaka Bay extensions and its relation with climatic evolution. *Quaternary Science Reviews* 29: 1863–1879.
- Kaspar F, Kuhl N, Cubasch U and Litt T (2005) A model–data comparison of European temperatures in the Eemian interglacial. *Geophysical Research Letters* 32: L11703. doi:10.1029/2005GL022456.
- Khodri M, Leclainche Y, Ramstein G, Braconnot P, Marti O and Cortijo E (2001) Simulating the amplification of orbital forcing by ocean feedbacks in the last glaciation. *Nature* 410: 570–574.
- Kistler R, Kalnay E, Collins W, Saha S, White G, Woollen J et al. (2001) The NCEP–NCAR 50-year reanalysis: Monthly means CD-ROM and documentation. *Bulletin of the American Meteorological Society* 82(2): 247–268.
- Laskar J (1990) The chaotic motion of the Solar System. A numerical estimate of the size of the chaotic zones. *Icarus* 88: 266–291.
- Lohmann K, Drange H and Bentsen M (2009) Response of the North Atlantic subpolar gyre to persistent North Atlantic oscillation like forcing. *Climate Dynamics* 32: 273–285.
- Loulergue L, Schilt A, Spahni R, Masson-Delmotte V, Blunier T, Lemieux B et al. (2008) Orbital and millennial-scale features of atmospheric CH₄ over the past 800,000 years. *Nature* 453: 383–386.
- Loutre MF and Berger A (2003) Marine Isotope Stage 11 as an analogue for the present interglacial. *Global Planetary Change* 36: 209–217.
- Lüthi D, Le Floch M, Bereiter B, Blunier T, Barnola J-M, Siegenthaler U et al. (2008) High-resolution carbon dioxide concentration record 650,000–800,000 years before present. *Nature* 453: 379–382.
- McManus J, Oppo D, Cullen J and Healey S (2003) Marine isotope stage 11 (MIS 11): Analogue for Holocene and future climate. *Geophysical Monograph* 137: 69–85.

- Meissner KJ, Weaver AJ, Matthews HD and Cox PJ (2003) The role of land-surface dynamics in glacial inception: A study with the UVic Earth System Model. *Climate Dynamics* 21: 515–537.
- Milankovitch M (1941) *Kanon der Erdbestrahlung und seine Anwendung auf das Eiszeiten-problem*. Belgrade: Royal Serbian Academy, Special Publication 132.
- Oleson KW, Dai Y, Bonan G, Bosilovich M, Dickinson R, Dirmeyer P et al. (2004) *NCAR Technical Description of the Community Land Model (CLM)*. NCAR/TN-461+STR.
- Parrenin F, Barnola J-M, Beer J, Blunier T, Castellano E, Chappellaz J et al. (2007) The EDC3 chronology for the EPICA Dome C ice core. *Climate of the Past* 3: 485–497.
- Peltier WR and Solheim LP (2004) The climate of the Earth at Last Glacial Maximum. Statistical equilibrium state and a mode of internal variability. *Quaternary Science Reviews* 23: 335–357.
- Raymo ME and Nisancioglu K (2003) The 41kyr world: Milankovitch's other unsolved mystery *Paleoceanography* 18(1): doi:10.1029/2002PA000791.
- Ruddiman WF (2003) The anthropogenic greenhouse era began thousands of years ago. *Climatic Change* 61: 261–293.
- Ruddiman WF (2006) Comment on 'Broecker WS and Stocker TL The Holocene CO₂ rise: Anthropogenic or natural?'. *EOS Transactions* 87: 352–353.
- Ruddiman WF (2007) The early anthropogenic hypothesis: Challenges and responses. *Reviews of Geophysics* 45: RG4001, doi:10.1029/2006RG000207.
- Ruddiman WF (2008) The challenge of modeling interglacial CO₂ and CH₄ trends. *Quaternary Science Reviews* 27: 445–448.
- Shackleton NJ, Berger A and Peltier WR (1990) An alternative astronomical calibration of the Lower Pleistocene timescale based on ODP Site 677. In: *The Late Cenozoic Ice Age. Transactions of The Royal Society of Edinburgh, Earth Sciences* 81: 251–261.
- Siegenthaler U, Stocker TF, Monnin E, Lüthi D, Schwander J, Stauffer B et al. (2005) Stable carbon cycle–climate relationship during the Late Pleistocene. *Science* 310: 1313–1317.
- Smith RD and Gent PR (2004) *Reference Manual for the Parallel Ocean Program (POP). Ocean Component of the Community Climate System Model (CCSM2.0 and 3.0)*. LAUR-02-2484, Los Alamos NM: Los Alamos National Laboratory.
- Spahni R, Chappellaz J, Stocker TF, Loulergue L, Hausammann G, Kawamura K et al. (2005) Atmospheric methane and nitrous oxide of the Late Pleistocene from Antarctic ice cores. *Science* 310: 1317–1321.
- Tarasov L and Peltier WR (1999) The impact of thermo-mechanical ice sheet coupling on a model of the 100 kyr ice-age cycle. *Journal of Geophysical Research* 104: 9517–9545.
- Thompson DWJ and Wallace JM (1998) The Arctic Oscillation signature in the wintertime geopotential height and temperature fields. *Geophysical Research Letters* 25: 1297–1300.
- Tzedakis PC, Raynaud D, McManus JF, Berger A, Brovkin V and Kiefer T (2009) Interglacial Diversity. *Nature Geoscience* 2: 751–755.
- Vavrus S and Waliser D (2008) An improved parameterization for simulating Arctic cloud amount in the CCSM3 climate model. *Journal of Climate* 21: 5673–5687.
- Vavrus S, Philippon-Berthier G, Kutzbach JE and Ruddiman WF (2011) The role of GCM resolution in simulating glacial inception. *The Holocene* (this issue). doi: 10.1177/0959683610394882.
- Vavrus S, Ruddiman WF and Kutzbach JE (2008) Climate model tests of the anthropogenic influence on greenhouse-induced climate change: The role of early human agriculture, industrialization, and vegetation feedbacks. *Quaternary Science Reviews* 27: 1410–1425.
- Vettoretti G and Peltier WR (2003a) Post-Eemian glacial inception. Part I: The impact of summer seasonal temperature bias. *Journal of Climate* 16: 889–911.
- Vettoretti G and Peltier WR (2003b) Post-Eemian glacial inception. Part II: Elements of a cryospheric moisture pump. *Journal of Climate* 16: 912–927.
- Vettoretti G and Peltier WR (2004) Sensitivity of glacial inception to orbital and greenhouse gas climate forcing. *Quaternary Science Reviews* 23: 499–519.
- Waelbroeck C, Labeyrie L, Michel E, Duplessy JC, McManus JF, Lambeck K et al. (2002) Sea-level and deep water temperature changes derived from benthic foraminifera isotopic records. *Quaternary Science Reviews* 21: 295–305.
- Young MA and Bradley RS (1984) Insolation gradients and the paleoclimatic record. In: Berger AL et al. (eds) *Milankovitch and Climate, Part 2D*. Norwell MA: Reidel, 707–713.